

TRAJECTORY GUIDANCE FOR MARS ROBOTIC PRECURSORS: AEROCAPTURE, ENTRY, DESCENT, AND LANDING

Ronald R. Sostaric⁽¹⁾, Carlie H. Zumwalt⁽²⁾, Eduardo García Llama⁽³⁾, Richard W. Powell⁽⁴⁾, Jeremy D. Shidner⁽⁵⁾

⁽¹⁾NASA Johnson Space Center, 2101 Nasa Parkway, Mailcode: EG5, Houston, TX, 77058, USA, Email: ronald.r.sostaric@nasa.gov

⁽²⁾NASA Johnson Space Center, 2101 Nasa Parkway, Mailcode: EG5, Houston, TX, 77058, USA, Email: carlie.h.zumwalt@nasa.gov

⁽³⁾G.B. Tech, 2101 Nasa Parkway, Mailcode: EG5, Houston, TX, 77058, USA, Email: eduardo.g.llama@nasa.gov

⁽⁴⁾Analytical Mechanics Associates, Langley Research Center, D205, Hampton, VA, 23681, USA, Email: richard.w.powell@nasa.gov

⁽⁵⁾Analytical Mechanics Associates, Langley Research Center, D205, Hampton, VA, 23681, USA, Email: jeremy.d.shidner@nasa.gov

ABSTRACT

Future crewed missions to Mars require improvements in landed mass capability beyond that which is possible using state-of-the-art Mars Entry, Descent, and Landing (EDL) systems. Current systems are capable of an estimated maximum landed mass of 1-1.5 metric tons (MT), while human Mars studies require 20-40 MT. A set of technologies were investigated by the EDL Systems Analysis (SA) project to assess the performance of candidate EDL architectures. A single architecture was selected for the design of a robotic precursor mission, entitled Exploration Feed Forward (EFF), whose objective is to demonstrate these technologies. In particular, inflatable aerodynamic decelerators (IADs) and supersonic retropropulsion (SRP) have been shown to have the greatest mass benefit and extensibility to future exploration missions. In order to evaluate these technologies and develop the mission, candidate guidance algorithms have been coded into the simulation for the purposes of evaluating system performance. These guidance algorithms include aerocapture, entry, and powered descent. The performance of the algorithms for each of these phases in the presence of dispersions has been assessed using a Monte Carlo technique.

1. INTRODUCTION

The development of the EFF study evolved from DRA 5.0 [1], the EDL-SA Year 1 Exploration-class study [2], and recent technology developments. Primary technology recommendations from the EDL-SA Year 1 Exploration study included Hypersonic Inflatable Aerodynamic Decelerators (HIADs), rigid aeroshells, and SRP. Since the conclusion of the Year 1 study, development has continued in NASA technology programs on the Inflatable Re-entry Vehicle Experiment's (IRVE) inflatable structure concept and ablator and insulator TPS materials. The continued development has led to an increase in maturity in

inflatable aeroshell technology. Previous work has shown the potential for large arrival mass reductions [2, 3, 4]. Additionally, the development of Autonomous Landing and Hazard Avoidance Technology (ALHAT) sensors for lunar missions prompted the desire for detailed simulation analysis of a similar system for Mars missions.

A single architecture class was selected for further examination with the objective of maximizing the number of feed forward technologies. The baseline architecture utilizes a dual HIAD system and SRP. The selected HIAD sizes were a 14 m diameter HIAD for aerocapture and 8 m HIAD for entry, based on a maximized landed payload mass optimization. EFF assumed a maximum launch mass capability of a Delta IV-H (7.2 MT) and an arrival velocity at Mars of 7.3 km/s, which corresponds to the 2024 opportunity.

The EFF mission design begins at Mars arrival. An aerocapture maneuver is used to slow the vehicle from a hyperbolic orbital energy to an elliptical energy by utilizing the atmospheric drag. The mission design assumes that a period of time is spent in orbit for checkout prior to entry. The aerocapture HIAD is jettisoned during this checkout phase. Prior to a de-orbit burn a second, smaller HIAD is inflated for use during entry. The de-orbit burn is then performed to initiate the entry sequence and drive the vehicle toward the desired entry interface state. Once the atmospheric drag forces have increased above a threshold, bank modulation is accomplished according to calculations provided by the entry guidance. Following the entry phase and the guidance-directed jettison of the heat shield, the SRP phase is initiated. During the SRP phase, the remaining vehicle velocity is reduced using a propulsive method with thrust magnitude and thrust direction calculations provided by the guidance. The guidance can dynamically retarget the landing site real-time to avoid hazards. The SRP phase culminates with safe touchdown on the Martian surface.

A simulation was developed and used to run initial integrated GNC performance and evaluate of SRP for Hazard Detection and Avoidance (HDA) and Terrain Relative Navigation (TRN). The EFF simulation includes 6DOF entry with Apollo entry guidance and a Linear Quadratic Regulator (LQR) bank angle controller and 3DOF powered descent with Apollo powered descent guidance and a pseudo controller. The ALHAT Extended Kalman filter (EKF) is also included in the simulation, but it does not include TRN update capability. However, statistically-based inertial measurement unit (IMU), star tracker, altimeter and velocimeter models are integrated in the simulation and utilized in the analysis.

2. AEROCAPTURE PERFORMANCE

The aerocapture portion of the EFF study was completed using four guidance algorithms; however, results included here are from the Hybrid Predictor-Corrector Aerocapture Scheme (HYPAS) [5] algorithm only. Details of the other algorithms can be found elsewhere [3]. The results shown here were generated using HYPAS in a 6DOF simulation with an LQR bank angle controller and an IMU to produce navigation states.

2.1 Hybrid Predictor-Corrector Aerocapture Scheme (HYPAS)

HYPAS is an analytical predictor-corrector algorithm that was developed and selected for the Aeroassist Flight Experiment, an aerocapture demonstrator mission that was canceled before launch. It has been used in numerous human and robotic exploration mission studies over the last 10 years for Earth and Mars, and has been proven to be robust for any moon or planet with an atmosphere and to a wide variety of lift-to-drag ratios (L/D), ballistic coefficients, atmospheres, entry conditions, and target orbits. It was considered for both the Mars Surveyor Program 2001 mission, and the Centre National d'Études Spatiales (CNES) Mars 2005 Sample Return Orbiter, and later, the CNES Mars 2007 Premier Mission. Unfortunately all these missions were canceled before launch. HYPAS targets a lifting vehicle through the atmosphere to a desired exit orbit apoapsis and inclination by using an analytically-derived guidance algorithm based on deceleration due to drag and altitude rate error feedback to determine the bank angle magnitude and the inclination error to determine bank direction.

2.2 Nominal Configuration Inputs

The primary nominal aerocapture parameters used

in the controllability analysis are given in Table 1.

Table 1. Nominal Aerocapture Parameters

Parameter	Value
Aeroshell Diameter	14m
Vehicle Diameter	4m
Ballistic Coefficient	33 kg/m ²
Lift-to-Drag Ratio (L/D)	0.25
Target Orbit	500km Circular
Entry Flight Path Angle	Case Dependent

These inputs are used to create the baseline EFF aerocapture configuration. The HIAD diameter was sized to satisfy a 3-sigma peak heat rate constraint of 50 W/cm² keeping in mind the minimum diameter constraint to prevent flow impingement. The heat rate constraint was based on the performance capability of an insulator thermal protection system [3]. Also the budgeted ΔV required to clean up the post-aerocapture orbit to match target orbit was constrained to 250 m/s. The clean up burn was modeled as a 3-burn maneuver that included (1) an apoapsis raise/lower maneuver, (2) a plane change maneuver, and (3) a periapsis raise maneuver.

The Monte Carlo dispersions used in this analysis are provided in Table 2, with additional dispersions placed on the IMU. These dispersions were chosen to be intentionally overly conservative in order to stress the guidance. A total of 8000 cases were run for each set of Monte Carlo results.

Table 2. Dispersions

Parameter	Nominal Value	Dispersion	Units	Dist.
Initial State				
Entry Flight Path Angle	Case Dependent	+/- 0.25	deg	Normal
Hyperbolic Velocity	5463.59	+/- 20	m/s	Normal
B-plane Angle	270.0	+/- 0.1	deg	Normal
Time of Flight	-30.0	+/- 2.0	sec	Normal
Atmospheric Uncertainties				
Dust Tau	0.45	0.1 to 0.9	[nd]	Uniform
Perturbation Seed Number	1	1 to 29999	[nd]	Integer
Density Multiplier	1.0	+/- 15%	[nd]	Uniform
Initial Attitude and Rate Uncertainties				

Alpha	-7 for L/D 0.10 -18.0 for L/D 0.25	+/- 0.25	deg	Normal
Beta	0.0	+/- 0.25	deg	Normal
Bank Angle	0.0	+/- 0.25	deg	Normal
Roll Rate BODY	0.0	+/- 0.10	deg/s	Normal
Pitch Rate BODY	0.0	+/- 0.10	deg/s	Normal
Yaw Rate BODY	0.0	+/- 0.10	deg/s	Normal
Aerodynamic Uncertainties				
CA Multiplier	1.0	0.9:1.1	[nd]	Normal
CN Multiplier	1.0	0.9:1.1	[nd]	Normal
CY Multiplier	1.0	0.9:1.1	[nd]	Normal
Mass Property Uncertainties				
XCG Bias Location	-0.22486	+/- 0.001	m	Normal
YCG Bias Location	0.0	+/- 0.001	m	Normal
ZCG Bias Location	0.175 for L/D 0.1 0.462 for L/D 0.25	+/- 0.001	m	Normal

2.3 Aerocapture Monte Carlo Results

Fig. 1 shows aerocapture heat rate and Fig. 2 shows ΔV results for the nominal EFF configuration given in Table 1, which uses an L/D of 0.25 and targets a post-aerocapture apoapsis of 500 km. The histogram of heat rate shows these cases met the 3-sigma peak heat rate requirement by not significantly exceeding 50 W/cm², and the maximum ΔV required to clean up the post-aerocapture orbit never approaches the 250 m/s budget. Additionally, the apoapsis values in this configuration form a very tight group around 500 km, which demonstrates that an L/D of 0.25 is sufficient to hit the target apoapsis for this entry speed and target orbit.

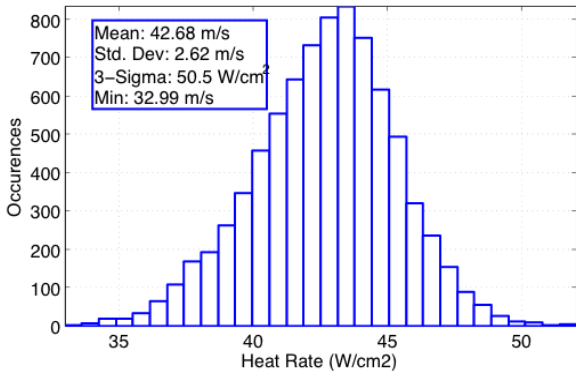


Fig. 1. Heat Rate for EFF-1 Aerocapture

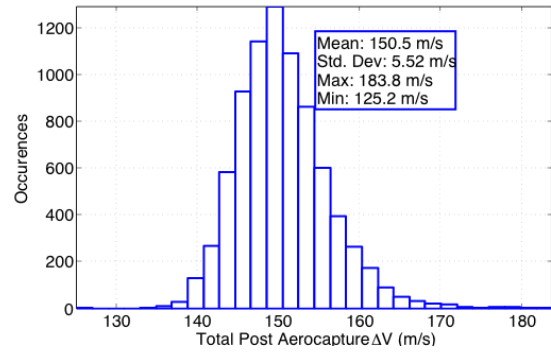


Fig. 2. Total ΔV for EFF-1 Aerocapture

Three trade studies were completed based on the nominal configuration to develop a further understanding of the aerocapture performance. These trade studies included considering a variation in L/D, the incorporation of a HIAD jettison maneuver, and a variation on post-aerocapture target orbit.

2.4 Trade 1 Results: L/D of 0.1 versus L/D of 0.25

Fig. 1 and Fig. 2 show that an L/D of 0.25 is sufficient to hit the target orbit apoapsis with the inputs and Monte Carlo dispersions listed in Table 1 and the references. Based on inquiries from both Year 1 and other technology programs (i.e. IRVE), a trade was performed to determine if the vehicle would still be able to meet the target apoapsis, given less available lift. Therefore, this study considers differences in performance associated with flying at an L/D of 0.25 and an L/D of 0.10.

Fig. 3 and Fig. 4 show the Monte Carlo results of the apoapsis and periapsis altitudes for an L/D of 0.10 and 0.25. The vehicle with the L/D of 0.10 is able to reach the target apoapsis, but inspection of the performance associated with individual lower L/D cases shows instances where the guidance is fully saturated. Guidance saturation occurs when the guidance must command maximum lift for the entire trajectory, leaving it no authority to fly out additional dispersions. To remedy this, the lateral corridor width is expanded for the lower L/D cases resulting in larger plane change maneuver ΔV , as shown in Fig. 5 and Fig. 6.

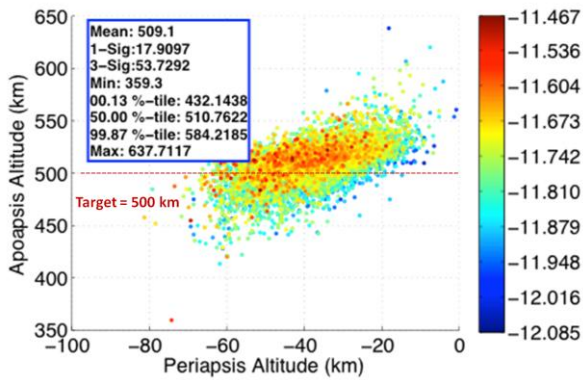


Fig. 3. Apoapsis Altitude vs Periapsis Altitude for L/D = 0.10

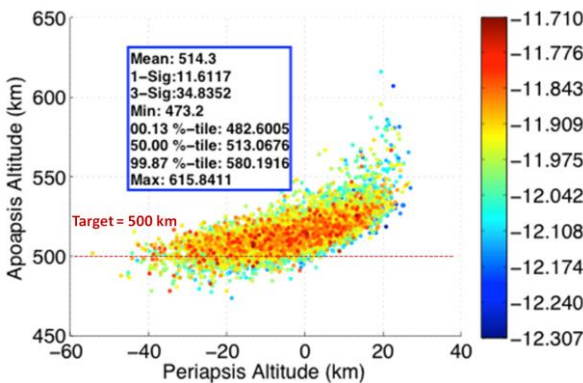


Fig. 4. Apoapsis Altitude vs Periapsis Altitude for L/D = 0.25

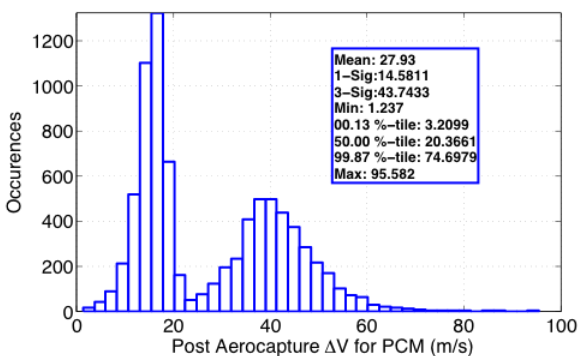


Fig. 5. Plane Change Maneuver ΔV for L/D of 0.10

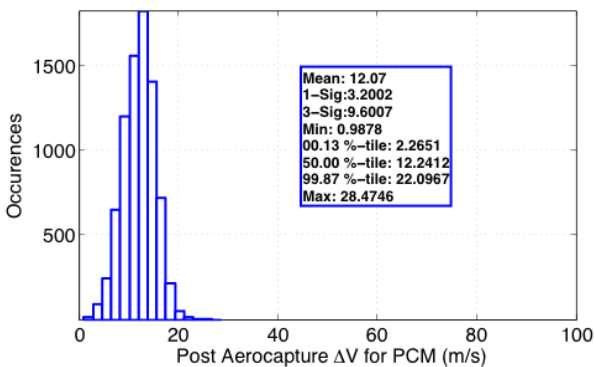


Fig. 6. Plane Change Maneuver ΔV for L/D of 0.25

This trade shows that aerocapture using a low L/D vehicle is feasible but will likely result in larger propellant use. Additionally, these results are specific to the EFF configuration described. Changes to target orbit or entry speed may result in cases that are unable to reach the target apoapsis for a lower L/D vehicle.

2.5 Trade 2 Results: Jettison versus No Jettison

Analyzing the results from the L/D trade study, specifically those from guidances that were unable to reach the target apoapsis for the lower L/D vehicle, led the team to consider alternate configurations to improve low L/D performance. Realizing that better performance might be achieved by adding an additional control parameter, consideration was given to analyzing the effect of jettisoning the HIAD atmospherically.

In an attempt to increase the ability of a specific guidance to hit the target orbit apoapsis, a subroutine was placed in the guidance, which uses the current navigation states to calculate apoapsis at each time step. Once that calculated apoapsis reaches a specified value, the HIAD is released and the vehicle changes from a lifting body to drag only. The jettison was modeled as a step function in the simulation, where at one time step the HIAD is attached and the next it is released. Jettisoning the HIAD in the atmosphere also allows aerodynamic forces to aid in separation. However, specific details of HIAD separation, such as 6DOF jettison dynamics or transitions, were not considered in this study. For this to be effective requires that there is a large ballistic number mismatch between the HIAD configuration and the spacecraft. This study had a ballistic number mismatch of about a factor of 12. No analysis was done to determine the lower bound of this parameter.

The disadvantage of jettisoning the HIAD in the atmosphere is that it only aids in hitting the apoapsis target when the guidance targets an apoapsis value below the desired target. This requires a much steeper flight path angle and can result in guidance saturation as well as higher heat rates. The advantage of jettisoning the HIAD is that it allows the vehicle to hit very close to the target apoapsis every time by essentially fixing the apoapsis value at the jettison point and allowing the vehicle to coast to a slightly lower apoapsis value, as illustrated in Fig. 7.

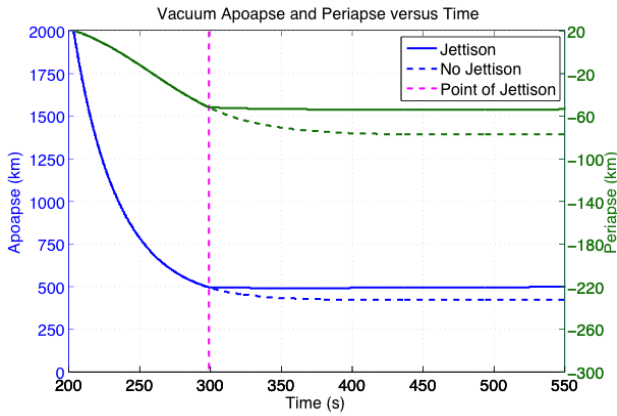


Fig. 7. Vacuum Apoapsis and Periapsis Altitude vs. Time With and Without HIAD Jettison

This trade study considers the effect of the jettison vs. no jettison for vehicles with an L/D of both 0.10 and 0.25. The first part of this study was performed for an L/D of 0.10, to determine what benefit the jettison maneuver might provide. Fig. 8 and Fig. 9 show the difference in apoapsis and periapsis values between the jettison and no jettison cases. By essentially fixing the apoapsis and periapsis values at the jettison point, the jettison maneuver allows the vehicle to hit the target with much better accuracy than the no jettison case. The smaller distribution in apoapsis and periapsis altitude values is reflected in Fig. 8 and Fig. 9. Consequently, jettisoning the HIAD also results in a reduction in the distribution of the periapsis raise maneuver ΔV shown in Fig. 10 and Fig. 11. The four points in Fig. 8 that are above 550 km are the cases where the calculated apoapsis value never reached the HIAD jettison condition, thus the HIAD remains attached for the duration of the flight.

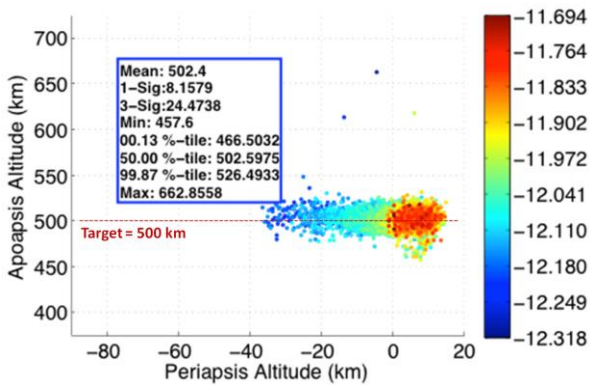


Fig. 8. L/D = 0.10: Apoapsis vs. Periapsis Altitude for Jettison

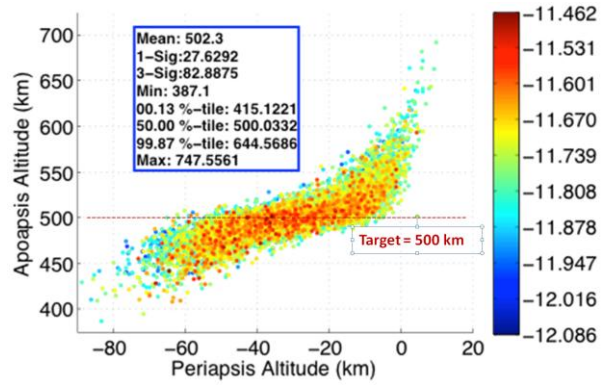


Fig. 9. L/D = 0.10: Apoapsis vs. Periapsis Altitude for No Jettison

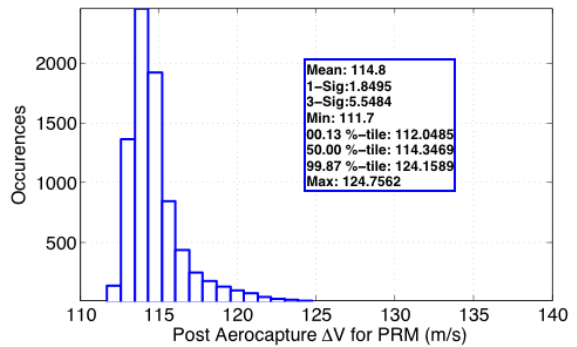


Fig. 10. L/D = 0.10: Periapsis Raise Maneuver ΔV for Jettison

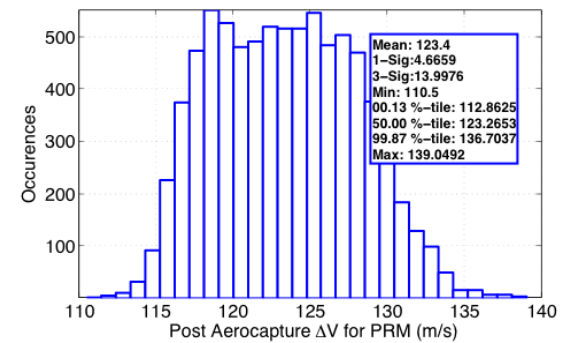


Fig. 11. L/D = 0.10: Periapsis Raise Maneuver ΔV , No Jettison

The second part of the study was performed for an L/D of 0.25 to determine if the benefits of the jettison maneuver persist at higher values of L/D. The observed effect of the jettison maneuver was a tightening of both the apoapsis and periapsis performance. This is illustrated in Fig. 12 and Fig. 13. However, the performance associated with the higher L/D no jettison cases suggest that no additional control parameter is necessary to help these cases reach their target orbit apoapsis.

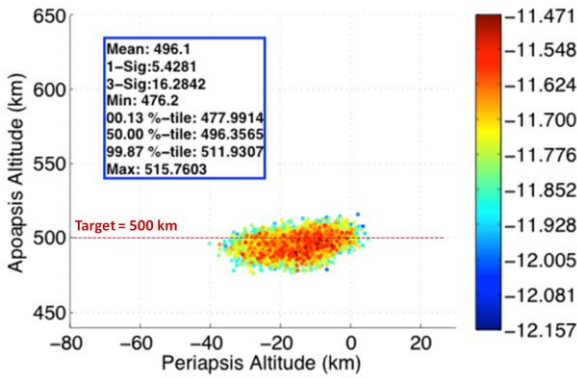


Fig. 12. L/D = 0.25: Apoapsis vs Periapsis Altitude for Jettison

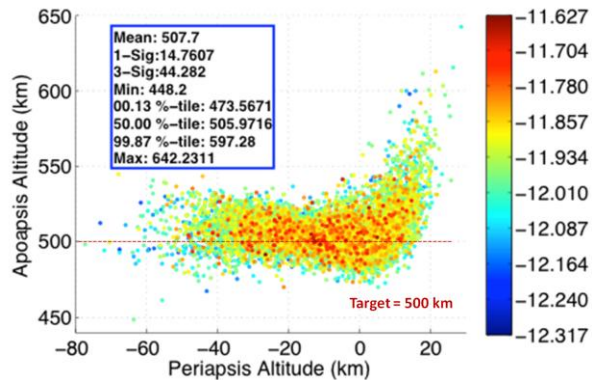


Fig. 13. L/D = 0.25: Apoapsis vs Periapsis Altitude for No Jettison

In summary, the jettison maneuver does improve the vehicle's ability to achieve a target orbit for any L/D. The necessity for the jettison maneuver becomes less critical at higher values of L/D and the decision to employ jettison for higher L/D vehicles will depend on mission specific requirements. Additionally, the modeling of the jettison maneuver is crude and factors such as HIAD separation and transitions would need to be considered if this concept were to be studied further.

2.6 Trade 3 Results: L/D of 0.25 with 500 km Circular Target Orbit Versus 1 sol Target Orbit

One final trade study was performed to determine the effect of changing the post-aerocapture target orbit for a vehicle with an L/D of 0.25. The apoapsis altitude associated with a 1 sol target orbit is 33,793 km, making it a much higher target and requires less energy (or ΔV) change compared to the 500 km circular orbit. The aerocapture maneuver performance is improved when more energy can be removed from the aeropass, therefore targeting a much higher apoapsis makes executing the aerocapture maneuver more difficult. For the higher apoapsis orbits, any error in velocity is associated with a large error in target apoapsis altitude,

which will require a larger ΔV to correct. Additionally, the lack of available corridor coupled with velocities that approach exit speeds creates the possibility of some cases becoming fly-bys.

Fig. 14 and Fig. 15 show a comparison of apoapsis and periapsis altitudes for the two target orbit cases. Noting the difference in plotted scales, the 500 km circular orbit has a much smaller distribution. However, the 1 sol cases spend less time in the atmosphere and are able to maintain much higher periapsis values. The benefit of that is evident in the ΔV required to clean up the periapsis value. The 500 km circular orbit requires almost ten times as much ΔV (average 125 m/s) as is required by the 1 sol orbit (average 13 m/s). For the full clean up burn (periapsis + apoapsis + wedge angle), the total ΔV required is on average 150 m/s for the 500 km circular orbit and 40 m/s for the 1 sol orbit.

In comparing the two target orbits, it is evident a large ΔV savings is achieved by changing to a target orbit with a higher apoapsis altitude but the propellant savings is at the cost of increased risk of fly-by or skip-out. The results of this trade are specific to the nominal inputs chosen for the EFF study and further work should be done to determine if the risk of skipping out at this high-energy orbit increases as the L/D or entry velocity decreases.

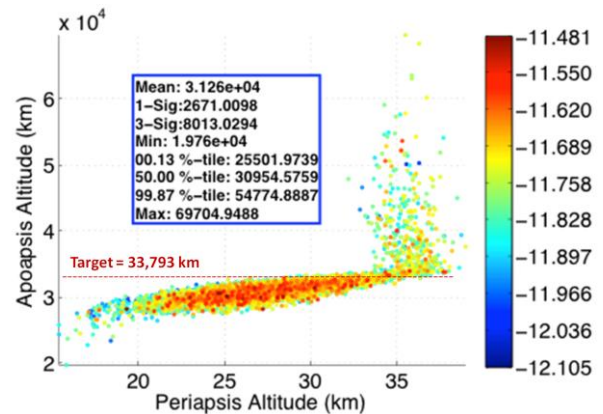


Fig. 14. Apoapsis vs. Periapsis Altitude for 1 sol target orbit

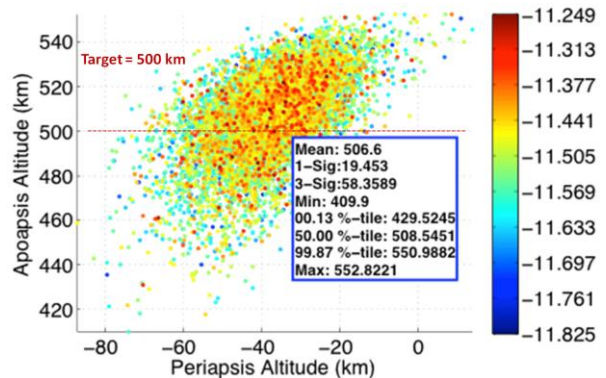


Fig. 15. Apoapsis vs. Periapsis Altitude for 500 km tgt.

2.7 Aerocapture Performance Conclusions

The nominal EFF aerocapture configuration using an L/D of 0.25 provides sufficient targeting capability while satisfying the constraints. For the L/D=0.10 case, the bank angle control was marginal (large number of trajectories saturated) with no HIAD jettison. Jettisoning the HIAD while in the sensible atmosphere indicates a capability to improve targeting. However, further modeling of the jettison maneuver is necessary to determine if it is a viable option. Additionally, targeting a higher post-aerocapture apoapsis shows significant reduction in clean-up ΔV , but these ΔV savings come at a higher risk of skip-out. Lastly, during the EFF study, the IRVE 4 team uncovered potential dynamics due to flexure at the joint between the rigid heat shield and the HIAD that need to be included in future systems analysis studies.

3. ENTRY GUIDANCE PERFORMANCE

The entry guidance used in the Study is an Apollo-derived entry guidance [6]. The Apollo-derived entry guidance algorithm is a terminal point controller that steers the vehicle to a HIAD separation point (range and velocity target) through bank commands using pre-derived influence coefficients with respect to errors about a nominal vertical L/D reference trajectory. This reference trajectory is defined by range-to-go, drag acceleration, and altitude rate as a function of relative velocity (Fig. 16).

The predicted range-to-go (R_p) is calculated as a function of drag (D) and altitude rate (\dot{r}) errors with respect to the nominal reference trajectory profile and the associated influence coefficients

$$R_p = R_{ref} + \frac{\partial R}{\partial D}(D - D_{ref}) - \frac{\partial R}{\partial \dot{r}}(\dot{r} - \dot{r}_{ref}) \quad (1)$$

The commanded vertical component of the lift-to-drag ratio is calculated as the addition of the reference vertical L/D plus a function of the difference between the actual and predicted range to go

$$\left(\frac{L}{D}\right)_{v,c} = \left(\frac{L}{D}\right)_{v,ref} + \frac{K3(R - R_p)}{\partial R / \partial (L/D)_v} \quad (2)$$

The commanded bank angle is then calculated as

$$\Phi_C = \cos^{-1}\left(\frac{(L/D)_{v,c}}{(L/D)}\right) \times K2_{roll} \quad (3)$$

where $K2_{roll}$ is the bank directional control (± 1). The sign of $K2_{roll}$ is reversed each time the target crossrange out-of-plane central angle exceeds the reversal criterion, which is a quadratic function of the relative velocity.

The partial derivatives of predicted range in Eq. 1 and Eq. 2 are the controller gains, which are derived using linear perturbation theory with the nominal reference trajectory by reverse integration of the differential equations adjoint to the linearized equations of motion. Optimized control gains for converging the dispersed trajectory are implemented in the guidance as tabular functions of relative velocity. Because of slow system and trajectory responses to guidance commands, performance is empirically enhanced by the use of the over-control gain $K3$ in Eq. 2 to improve range convergence behavior.

To minimize disturbance of downrange control near the target, bank reversals are inhibited below a certain relative velocity magnitude. If the bank command is not in the same direction as the target at this point, then a final reversal is commanded prior to setting the inhibit flag. After that, a heading control phase is initiated in which the bank command is defined by

$$\Phi_C = \tan^{-1}\left(\frac{C_r}{D_r}\right) \times K4 \quad (4)$$

where $K4$ is the overcontrol gain for the heading control phase and where C_r and D_r are the crossrange and downrange to the target, respectively.

A variable bank reference trajectory was selected (see Fig. 16). It is known that variable bank reference trajectories result in smaller velocity at a given final altitude than constant bank trajectories. A simple variable bank profile that is known to perform well is a linear ramp followed by a constant value [7], and this is the type of trajectory that was chosen for this study.

Since the Apollo guidance controls bank angle within a corridor about the reference profile to converge the terminal range, it is desirable to design this profile to provide as much margin as possible from the vehicle maneuver capability limits to accommodate dispersions. This means that bank angles of the nominal reference trajectory should allow sufficient margin so that, in a dispersed simulation, the guidance is able to retain sufficient capability to converge the range without bank angle saturation. Experience has shown that the nominal bank limits can be reasonably estimated from the atmospheric density ρ and C_d percentage dispersions using the expression $\Phi_{Cmin} = \cos^{-1}(100\% - \rho\% - C_d\%)$. In the reference trajectory, the bank value of 45° for the constant bank phase is based on this expression [7]. The nominal final altitude of the reference trajectory is determined such that all the powered descent dispersed cases are successful.

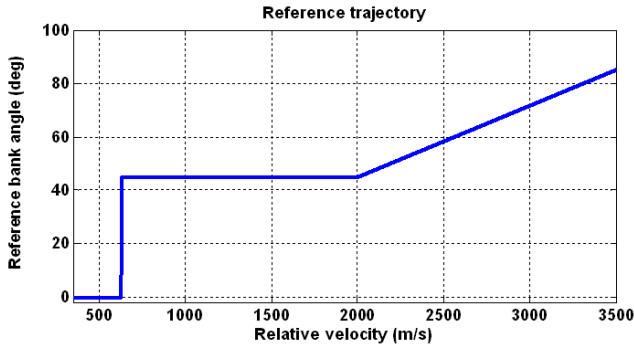


Fig. 16. Reference Bank Profile

The performance was assessed using 6DOF Monte Carlo analysis comprised of 8000 runs with simple propagator navigation (Fig. 17 and Fig. 18). Downrange error is not shown because the simulation end condition is based on range, thus, the downrange error is very small at separation. Downrange error at engine initiation is within ± 200 m.

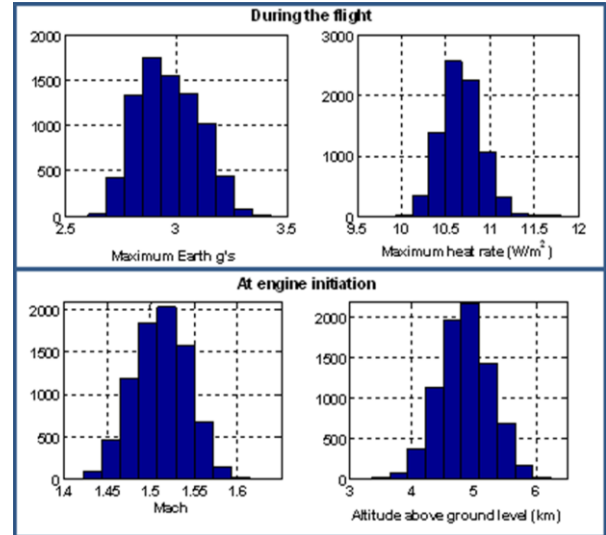


Fig. 18. Entry Performance Summary: Histogram of Maximums and Conditions at Engine Initiation

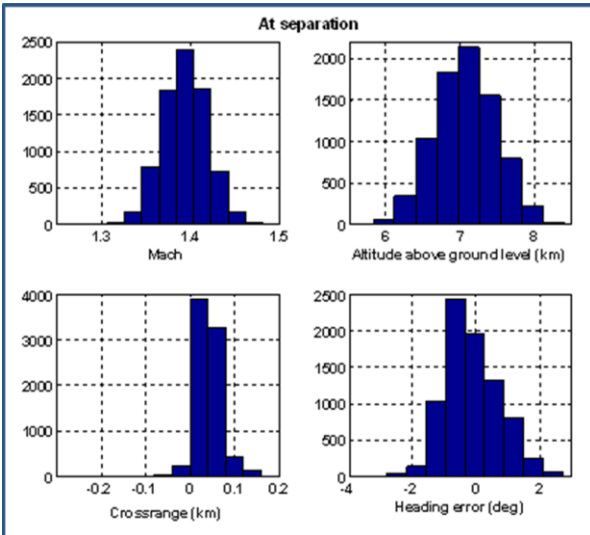


Fig. 17. Entry Performance Summary: Histogram of Conditions at Separation

Using the dispersions defined in Table 2, the design of the entry guidance is capable of achieving the engine initiation conditions such that all the powered descent dispersed cases can be landed successfully. However, this design of the entry guidance should not be considered as a final design. There is room for improvement by fine tuning and improving the guidance parameters that affect the performance (reference profile, over-control settings, initial flight path angle, drag acceleration and L/D filter time constants and the drag and altitude controller gain scale factors).

4. POWERED DESCENT PERFORMANCE

The objective of the powered descent is to steer the vehicle to a controlled touchdown using the main propulsion engines. The following assumptions were made for the powered descent analysis:

- Apollo LM-derived guidance (2nd order polynomial in acceleration) [8]
- Initial states for powered descent from entry Monte Carlo results
- 3-DOF pseudo control with 20 deg/sec and 5 deg/sec² attitude limits (the pseudo controller mimics a 6 DOF simulation by converting the displacement error signal to an instantaneous acceleration, which is then integrated within the specified acceleration and rate limits)
- Perfect navigation

- Target touchdown velocity is 1 m/s vertical, 0 m/s horizontal
- Fly out all position error prior to touchdown
- 8000 case Monte Carlo
- Dispersions as given in Table 2

Fig. 19 shows a depiction of the powered descent phase. The powered descent begins just after a 15 sec freefall phase, which is used to simulate a transition from entry and jettison of the aeroshell. The powered descent is about an 80 sec burn over the last 4-7 km of descent altitude. The last 5 m of altitude is simulated as a constant velocity phase with a 1 m/s descent rate.

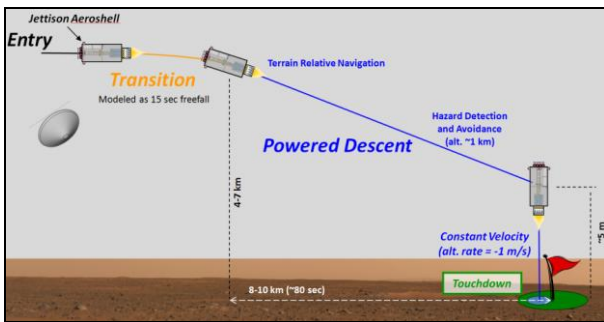


Fig. 19. Powered Descent Nominal Trajectory

Fig. 20 and Fig. 21 show the initial conditions for the powered descent. These conditions are inherited from the entry and are essentially a function of the entry trajectory design. The altitude range is 4-7 km, the Mach number range is 1.4 – 1.8, and the downrange is 8-9 km.

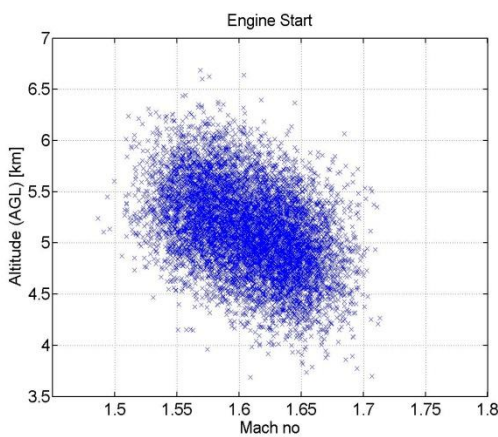


Fig. 20. Altitude vs Mach Number at the Start of Powered Descent

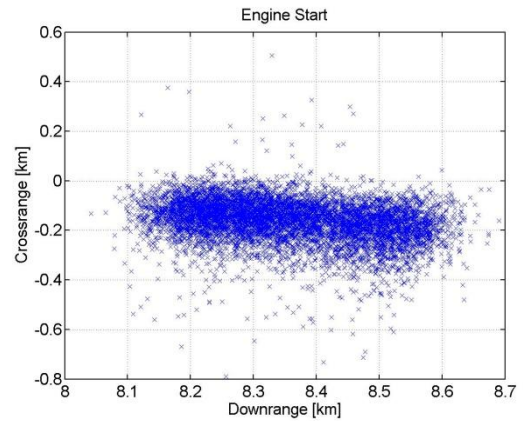


Fig. 21. Crossrange vs Downrange at the Start of Powered Descent

Recognizing that the entry trajectory design has significant effect on powered descent performance, an effort was made to choose the entry termination point such that all dispersions at the start of powered descent could be removed with the minimum amount of fuel. The current design achieves touchdown with essentially zero altitude/velocity error. If the termination altitude for entry were lower, some cases would not be able to successfully achieve the target touchdown conditions due to maximum thrust limitations. If entry were to end at higher altitude, additional fuel would be needed for powered descent.

Table 3 shows the propellant usage statistics at touchdown. The 99.87th percentile value for propellant consumed was 870.5 kg. The 0.13th percentile value for propellant remaining at touchdown was 249.5 kg. Given the current dispersions and entry performance, the powered descent has sufficient propellant margin. Further study showing the effect of navigation on powered descent is discussed in the EDL-SA Report [3, 4].

Table 3. Propellant Usage Statistics at Touchdown

	Propellant Consumed kg	Propellant Remaining kg
Mean	893.0	226.9
1-sigma	8.1	8.1
3-sigma	24.3	24.3
0.13%-tile	872.9	208.3
50.00%-tile	893.5	226.5
99.87%-tile	911.7	247.1

4.1 Terrain Relative Navigation (TRN) and Hazard Detection and Avoidance (HDA) Feasibility

A brief investigation of feasibility of both TRN and HDA was undertaken. TRN works over a wide range of altitude and velocity and is possible anytime sensor measurements can be taken and a high-quality map of the terrain is available. There are two basic forms of TRN: optical TRN, which uses optical cameras in the visible spectrum; and active TRN, which uses an altimeter, flash lidar, or other active sensor. Fundamentally, all that is needed is to ensure that this sensor has a view of the surface and that the navigation has a reasonable estimate of the vehicle's inertial position. Since the attitude profile during the first 60 sec is well off of the vertical (see Fig. 22), it can reasonably be assumed that TRN measurements can be taken and that TRN is feasible.

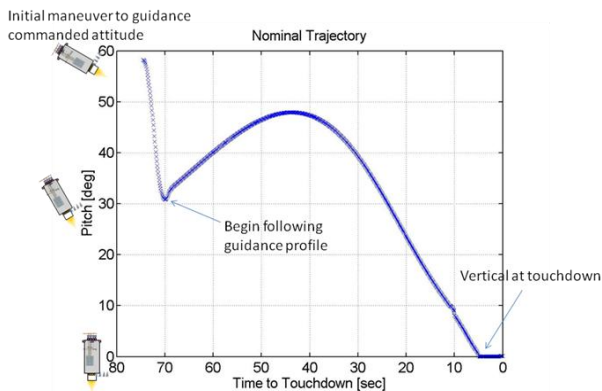


Fig. 22. Pitch Profile During Powered Descent

Feasibility for HDA is more complex to demonstrate than for TRN. The flash lidar must scan the landing area, so it requires a line of sight to the landing area at the correct time during the descent. The lidar will be designed for optimum performance at a particular slant range from the landing site. The scan must occur at this distance to ensure that sufficient resolution is achieved and the full landing area can be scanned.

An initial analysis of the nominal trajectory shows that HDA is feasible for the nominal trajectory by looking out the rear facing (uprange) side of the vehicle (in the same direction in which TRN would occur) at an altitude of 1 km. Fig. 23 define the angles of interest. The look angle describes the angle between the body x-axis (the long axis) and the line of sight to the target. Fig. 24 depicts the time history of these angles for the nominal trajectory. The vehicle passes through 1 km altitude at $t=28$ sec to touchdown. The look angle at this point is -14 deg, meaning the lidar would have to be mounted such that the landing site would be viewing along the back side of the vehicle, rather the

forward facing side. However, in dispersed cases the look angle may be close to zero and the distribution of the look angle may be both positive and negative at the time of the scan. This would require two sensors, one on each side of the vehicle. The trajectory can likely be redesigned such that all look angles are positive, for a minimal cost in additional propellant usage – and would only require one HDA sensor. Further investigation is needed before a conclusive determination can be made regarding HDA feasibility.

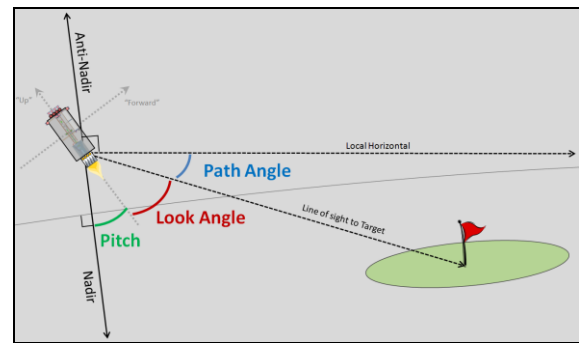


Fig. 23. Definition of Angles of Interest During Powered Descent

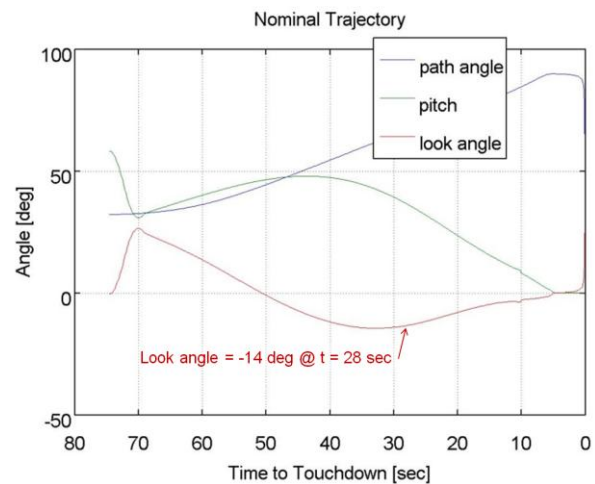


Fig. 24. Nominal Trajectory Angles of Interest

5. CONCLUSIONS

A Monte Carlo assessment of guidance and trajectory performance of a large-mass robotic precursor mission has been completed. This mission would demonstrate a 14 m HIAD for aerocapture, an 8 m HIAD for entry, and supersonic retropropulsion in the less than Mach 2 range. Additionally, it includes a demonstration of TRN and HDA techniques and sensors being developed by ALHAT. The results show an initial estimate of the system performance and serve as a starting point for future large-mass robotic precursor mission development work.

6. ACKNOWLEDGEMENTS

The authors would like to acknowledge their EDL-SA teammates. In particular, Alicia Dwyer Cianciolo served at the EFF Study Lead and strongly influenced the overall direction of the study. Jody Davis did much of the work in putting together the POST2 simulation which was used to obtain the results in this paper. Eric Queen developed the 6DOF LQR bank angle controller, an aerocapture guidance concept, and performed control analysis for aerocapture. David Way also developed an aerocapture guidance concept. Thanks to all of the above for their contributions to the project and their influence on the work discussed here.

7. REFERENCES

1. Drake, B. G., editor., "Human Exploration of Mars Design Reference Architecture 5.0," s.l. : NASA-SP-2009-566, July 2009.
2. Dwyer Cianciolo, A. M., et al. "Entry, Descent and Landing Systems Analysis Study: Phase 1 Report." NASA/TM-2010-216720.
3. Dwyer Cianciolo, A. M., et al. "Entry, Descent and Landing Systems Analysis Study: Phase 2 Report on Exploration Feed Forward Systems." NASA/TM-2011-217055, February 2011.
4. Dwyer Cianciolo, A. M. (ed.), "Entry, Descent and Landing Systems Analysis: Exploration Feed Forward Internal Peer Review Slide Package", NASA/TM-2011-217050, February 2011.
5. Cerimele, C.J. and Gamble, J.D., "A Simplified Guidance Algorithm for Lifting Aeroassist Orbital Transfer Vehicles," AIAA-85-0348, AIAA 23rd Aerospace Sciences Meeting, Reno, NV, January 1985.
6. Moseley, P. E., "The Apollo Entry Guidance: A Review of the Mathematical Development and Its Operational Characteristics", TRW Note No. 69-FMT-791, TRW, December 1, 1969.
7. Mendeck, Gavin and Carman, Gilbert, "Guidance Design for Mars Smart Landers Using the Entry Terminal Point Controller", AIAA-2002-4502. AIAA Atmospheric Flight Mechanics Conference and Exhibit, Monterey, California, Aug. 5-8, 2002.
8. Sostaric, R. and Rea, J., "Powered Descent Guidance Method for the Moon and Mars", AIAA GN&C/Flight Mechanics Conference, San Francisco, CA, August 2005.